Energy Exchange and Temperature of Aerosols in the Earth's Atmosphere (0–60 km)

GIORGIO FIOCCO[1]

Università, Istituto di Fisica, Roma, Italy

GERALD GRAMS

National Center for Atmospheric Research[2] Boulder, Colo. 80307

ALBERTO MUGNAI

Università, Istituto di Fisica, Roma, Italy

(Manuscript received 20 February 1975, in revised form 20 July 1976)

ABSTRACT

A previous analysis (Fiocco *et al.*, 1975) of the energetic equilibrium of small particles in the earth's upper atmosphere is extended to the 0–60 km region. The analysis is based on establishing a balance among the energy absorbed from solar and planetary radiation fields, the energy radiated by the particles, and the sensible heat exchanged through collisions with the ambient gas. The planetary radiation field is calculated as a function of altitude and includes radiation from the surface as well as emission and absorption by the infrared bands of CO_2, O_3 and H_2O. The various energy terms change as a function of radius and altitude of the particles, season, time of day and the earth's albedo. Thus aerosols may heat or cool the atmosphere and their temperature may differ from the ambient gas temperature. Maximum and average values for the heating rates induced by the particles into the ambient gas are computed for summer and winter 45°N conditions.

1. Introduction

In a related paper (Fiocco, Grams and Visconti, 1975; hereafter referred to as FGV), the energetic equilibrium of aerosol particles in the Earth's atmosphere has been investigated and results have been presented for the 50–110 km region. Aerosols absorb energy from the solar and planetary radiation fields, exchange energy by collisions with the ambient gas, and emit thermal radiation. When changes in phase are possible, they also cause the aerosols to lose or acquire latent heat. Interaction with the radiation field is a function of the size and refractive index of the particles and of the spectral density and anisotropy of the radiation. The heat exchanged through collisions is a function of the temperature and density of the ambient gas and of the temperature of the particles. Thus the equilibrium conditions for a given particle size and composition are a function of the altitude, as well as the time of day, season, and planetary albedo.

As a result of such equilibrium, the particle temperature T_p can be substantially different from the ambient gas temperature T_g. The effect is large above 60 km, where differences $T_p - T_g$ in excess of 100 K can be obtained in daytime—as demonstrated by FGV. These differences may account for a substantial increase in the sublimation rates of certain species (Fiocco and Visconti, 1973), for a reduction in the altitude interval where ice particles can exist in the mesosphere (Grams and Fiocco, 1976), and possibly for an increase in the catalytic efficiency of aerosols in chemical reactions.

The ratio between the different terms of the equation of energetic equilibrium changes with altitude and particle size. Thus, there are changes in the fraction of energy absorbed from the radiation field that goes directly into the sensible heat of the ambient gas because of molecular collisions. In this way, particles in different size ranges and at different heights may vary in their effectiveness for heating and cooling the ambient gas.

In FGV, results were shown for the earth's upper atmosphere (50–110 km). The flux of planetary thermal radiation was accounted for in a straightforward manner, using infrared radiance data obtained by the infrared interferometer spectrometer (IRIS) on the Nimbus 4 meteorological satellite (Kunde *et al.*, 1974). This procedure was considered adequate above 50 km, but at lower heights atmospheric absorption and

[1] Part of this research was carried out as a Visiting Senior Fellow of the Advanced Study Program, National Center for Atmospheric Research.

[2] The National Center for Atmospheric Research is sponsored by the National Science Foundation.

Unauthenticated | Downloaded 11/28/21 12:39 AM UTC

emission have the effect of significantly modifying, as a function of altitude, the spectral density distribution and the anisotropy of the radiation incident on the particle. Furthermore, large variations in heating rates are obtained in the lower atmosphere even though temperature differences $T_p - T_g$ are small. In this paper, the analysis of FGV is extended to take into account the altitude dependence of the planetary thermal radiation; the energy equilibrium computations are carried out from ground level to an altitude of 60 km.

2. Analysis

The analysis is based on establishing the equilibrium condition for a spherical aerosol particle of radius r; i.e.,

$$P_{A,\odot} + P_{A,\text{pla}} - P_E - P_C = 0, \tag{1}$$

where $P_{A,\odot}$ is the solar radiation power absorbed by the particle, $P_{A,\text{pla}}$ the planetary radiation power absorbed by the particle, P_E the thermal power radiated by the particle, and P_C the power lost by the particle because of collisions with the ambient gas; all units are in watts. In the equilibrium calculations, it is assumed that the particle does not change size or state; therefore, effects of latent heat exchange are omitted in Eq. (1). The analysis of the various equilibrium terms, with the exception of $P_{A,\text{pla}}$, follows that of FGV and is summarized as follows.

The solar radiation power absorbed can be expressed as

$$P_{A,\odot} = \pi r^2 (1 + 2A \cos\chi) \int_0^\infty Q_{\text{abs}} F_\odot(\lambda) d\lambda, \tag{2}$$

where χ is the solar zenith angle, Q_{abs} the efficiency factor for absorption and $F_\odot(\lambda)$ the solar spectral flux (W m^{-2} μm^{-1}) at the wavelength λ outside the earth's atmosphere (Thekaekara, 1973). The spectral variation of the complex refractive index, as specified by the synthetic aerosol model of Ivlev and Popova (1973), has been used for the computation of Q_{abs} by using Mie theory. The planetary albedo A is assumed to be a surface effect that is independent of wavelength; thus, effects of the earth's atmosphere on solar radiation such as absorption and multiple scattering have not been taken directly into account in the present investigation.

The planetary radiation power $P_{A,\text{pla}}$ is expressed as

$$P_{A,\text{pla}} = \pi r^2 \int_0^\infty Q_{\text{abs}} F_{\text{pla}}(\lambda) d\lambda, \tag{3}$$

where $F_{\text{pla}}(\lambda)$ is the spectral flux of planetary radiation incident on the particle due to emission from the planetary surface and to atmospheric absorption and emission; $F_{\text{pla}}(\lambda)$ will be considered in more detail later in this section.

The thermal power radiated by the particle is

$$P_E = 4\pi r^2 \int_0^\infty Q_{\text{abs}} F_\lambda(T_p) d\lambda, \tag{4}$$

where $F_\lambda(T_p)$ represents the Planck function in flux units (W m^{-2} μm^{-1}) at the wavelength λ and at the temperature of the particle T_p.

The power lost because of collisions can be written as

$$P_C = n_c a (E_p - E_g) = 2 n_g r^2 (2\pi K_B T_g / m_g)^{\frac{1}{2}} \times a(c_v m_g + \tfrac{1}{2} K_B)(T_p - T_g), \tag{5}$$

where $n_c = 2 n_g r^2 (2\pi K_B T_g / m_g)^{\frac{1}{2}}$ is the number of molecules that collide with the particle per second; c_v is the atmospheric specific heat at constant volume; n_g, m_g and T_g are, respectively, the number density, the mass, and the temperature of the ambient atmospheric molecules; and K_B is Boltzmann's constant. In deriving the above expression for P_C, we used the concept of the accommodation coefficient described by Kennard (1938), i.e.,

$$a = (E - E_g)/(E_p - E_g), \tag{6}$$

where $E_g = (c_v m_g + \frac{1}{2} K_B) T_g$ is the mean energy per molecule transported toward the surface of the particle from a gas in thermal equilibrium at the temperature T_g, E is the actual mean energy per molecule after colliding with the particle, and $E_p = (c_v m_g + \frac{1}{2} K_B) T_p$ is the mean energy per molecule transported by a gas in thermal equilibrium at the particle temperature T_p.

According to Kennard, the value of the accommodation coefficient ranges from about 0.1 to unity. Most of the calculations presented in this paper have been made with $a = 1$; a discussion of the effect of using different values is presented later.

The analysis outlined so far is the same as in FGV; the reader is referred to that paper for further details. In FGV, the spectral flux of planetary radiation $F_{\text{pla}}(\lambda)$ was accounted for in a straightforward manner, using Nimbus 4 IRIS measurements. In order to extend the model to lower altitudes, we specified the planetary spectral flux as a function of the altitude of the particle z_p by radiative transfer calculations based on procedures developed and published by other authors.

To compute $P_{A,\text{pla}}$ we divided the spectral region 4.5–62.5 μm into several intervals i of spectral width $\Delta\lambda_i$, and approximated (3) by the following expression:

$$P_{A,\text{pla}} = \pi r^2 \sum_i F_i(z_p) \int_{\Delta\lambda_i} Q_{\text{abs}} d\lambda, \tag{7}$$

where the average planetary flux $F_i(z_p)$ in each spectral interval is given by

$$F_i(z_p) = 2\pi \int_0^\pi I_i(z_p, \theta) \sin\theta d\theta. \tag{8}$$

In the above expression, θ is the zenith angle of the incident radiation, and the average radiation intensity over each interval I_i (z_p, θ) [W m^{-2} sr^{-1} μm^{-1}] is determined with the help of the equation of radiative transfer, whose solution gives, for the upward(+) and

Unauthenticated | Downloaded 11/28/21 12:39 AM UTC

downward(−) intensities

$$I_i^+(z_p,\theta)=B_i(T_{sfc})\mathcal{T}_i(z_p,0,\theta)+\int_{\mathcal{T}_i(z_p,0,\theta)}^{1}B_i[T_g(z')]d\mathcal{T}_i(z_p,z',\theta)$$

$$I_i^-(z_p,\theta)=B_i[T_g(Z)][\mathcal{T}_i(z_p,Z,\theta)-\mathcal{T}_i(z_p,z_{top},\theta)]+\int_{\mathcal{T}_i(z_p,Z,\theta)}^{1}B_i[T_g(z')]d\mathcal{T}_i(z_p,z',\theta). \quad (9)$$

Here $B_i(T)$ represents the Planck function in intensity units (W m^{-2} sr^{-1} μm^{-1}) at the temperature T in the spectral interval i, where it is regarded as constant; T_{sfc} is the earth's surface temperature; and $\mathcal{T}_i(z_p,z,\theta)$, the mean transmissivity of the atmosphere between the level z_p and every level z, is a function of the spectral interval i and of the direction θ. Moreover, the atmospheric radiation emitted by the molecules above the assumed upper boundary Z is approximated by that emitted by a uniform layer at the top of the atmosphere, whose thickness $z_{top}-Z$ is taken to be the scale height at the altitude Z.

To compute the transmissivities, we considered the most important absorption bands in the range 4.5–62.5 μm. In particular, we used the Curtis-Godson approximation and the results and the procedures of Rodgers and Walshaw (1966) for the 6.3 μm and the rotational bands of H_2O; for the 15 μm band of CO_2, we used an empirical fit to the measured equivalent width of the whole band, proposed by the same authors; for the 9.6 μm band of O_3, we used the four-parameter approximation and an empirical fit to the measured integrated absorption proposed by Rodgers (1968); finally, we used the Curtis-Godson approximation and the data of Bignell (1970) in the linear form used by Cox (1973) for the 8–15 μm continuum region.

The temperature and pressure dependence with altitude and with the season is according to the U. S. Standard Atmosphere Supplements, 1966. The midlatitude O_3 model is also taken from that publication. The H_2O distribution up to 10 km is calculated according to the values of relative humidity taken from the above publication; at 13 km and above, a mass mixing ratio of 8 parts per million (ppm) is assumed; values at intermediate heights are calculated by assuming a constant H_2O scale height between the above-mentioned levels. For CO_2, a constant value of the volume mixing ratio equal to 316.5 ppm is taken.

The computations have been carried out for summer and winter at 45°N; values of $Q_{abs}(r,\lambda)$ and values of $F_i(z_p)$ were computed and then used to solve Eq. (1) numerically, following the procedure described in FGV. The values of P_C at each particle size were also converted into heating rates dT_g/dt (K day^{-1}) with the aid of the expression

$$\frac{dT_g}{dt}=\frac{3\nu P_C}{4\pi r^3\rho_p c_p}, \quad (10)$$

where ρ_p is the mass density of the aerosol material (we assume $\rho_p=1$ g cm^{-3}), c_p is the specific heat of air at constant pressure, and the aerosol mass mixing ratio ν has been taken constant with respect to altitude and particle radius, $\nu=1$ part per billion (ppb). The dependence on size and altitude of T_p, P_C and dT_g/dt has been studied for the two seasons, for different times of day, and for different values of the planetary albedo. Also, we have integrated the hour-by-hour values of the heating rate to obtain the corresponding daily average heating rates.

3. Aerosol temperatures

Fig. 1 shows values of the temperature difference T_p-T_g as a function of altitude between 0 and 60 km, and of size between 0.01 and 10 μm radius. Parts (a) and (b) show values of the difference at midday for summer and winter, respectively; similarly, parts (c) and (d) show nighttime differences for summer and winter. The albedo values for the midday results are taken as 0.3 for the summer and 0.5 for the winter. These values are representative for the average seasonal conditions at 45°N (Raschke *et al.*, 1973).

While differences T_p-T_g have been shown by FGV to be in excess of 100 K in the region above 60 km, maximum midday values are smaller than 1 K below about 50 km, and smaller than 0.01 K below about 10

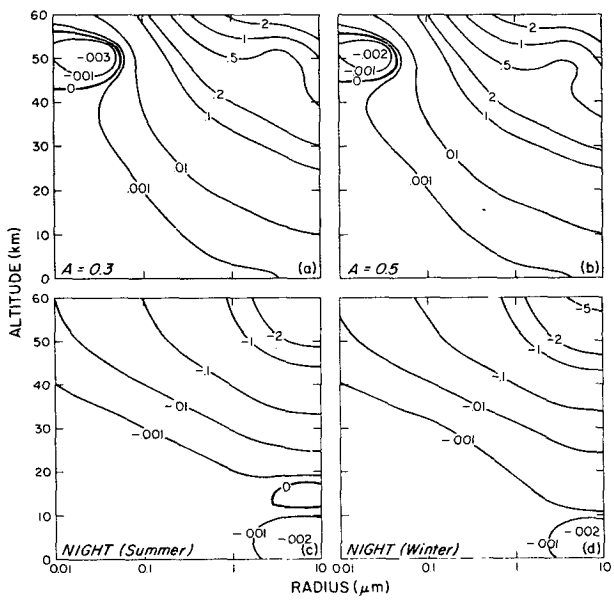

FIG. 1. Temperature differences, T_p-T_g, for aerosols with the complex refractive index proposed by Ivlev and Popova (1973) at midday for (a) $A=0.3$ in summer and (b) $A=0.5$ in winter, and at nighttime for (c) summer and (d) winter.

Unauthenticated | Downloaded 11/28/21 12:39 AM UTC

km. The sign of the difference is an indicator of whether the particle adds or removes heat from the ambient gas by conduction. It can be seen that at midday, with the exception of a limited region near 50 km, such differences are always positive; that is, particles deposit heat by conduction into the gas. On the other hand, with the exception of a limited region just above the tropopause for summer conditions, particles remove heat at night.

In these computations, the energy lost or gained by phase changes has not been taken into account. In situations where conditions for water vapor condensation exist, the exchange of latent heat could substantially modify the equilibrium conditions; the analysis should then be replaced by a dynamical model whereby the particles are allowed to change in size. On the other hand, in such a case the particles could no longer be considered homogeneous spheres and their radiative properties would change. These conditions are likely to be of importance, however, only in the troposphere. Analyses of the growth of particles in a radiation field have been carried out by Shifrin and Zolotova (1966, 1971) and by Higuchi (1969).

4. Energy exchange

Fig. 2 shows the variation with height of the power terms entering into Eq. (1) for particles with $r=0.3$ μm for summer and winter. Midday and nighttime profiles are shown. In our relatively simple model, the solar radiation terms $P_{A,\odot}$ are constant with height, but they change during the day as the solar zenith angle changes; they disappear, of course, at night. The planetary radiation terms $P_{A,\text{pla}}$ are a function of height and season but do not change between day and night. The power P_C lost by the particles because of collisions with the ambient gas is always negative at night, but strongly positive in the daytime. The infrared emitted power P_E changes slightly between night and day, and only in the upper regions. It is clear that the longwave radiation terms—the power $P_{A,\text{pla}}$ adsorbed from the planetary field and the power P_E emitted by the particle—do not balance each other; thus the collisional term P_C will have a significant role in the energy exchange process.

The exchange of sensible heat by collision with gas can be represented also in terms of the heating rate. Results are shown in Figs. 3, 4 and 5 for a constant mass mixing ratio of aerosols, $\nu=1$ ppb, as in the FGV analyses. Figs. 3 and 4 show midday heating rates in summer and winter, respectively, for albedo values $A=0.08$, 0.3, 0.5 and 0.7, and for particle radii between 0.01 and 10 μm. The value $A=0.08$ is thought to be typical of the ocean surface and $A=0.7$ is typical for snow or clouds; $A=0.3$ is the global annual average (also typical for summertime at 45°N), and $A=0.5$ is a representative value for winter at 45°N. An increase in heating rate with increasing albedo is quite evident; in the lower stratosphere, the heating rate doubles between the smallest and largest albedo values. Around the altitude of 50 km, negative heating rates are obtained for particles with radii smaller than 0.1 μm, with the exception of the results for the highest albedo

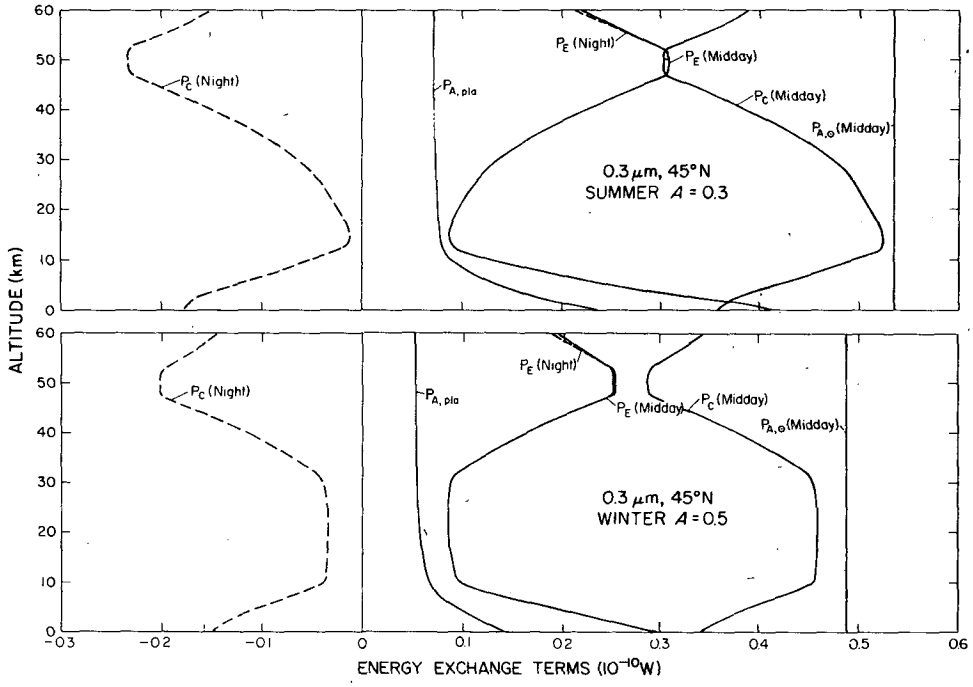

FIG. 2. Behavior of energy exchange terms in Eq. (1) for aerosols with 0.3 μm radius.

Unauthenticated | Downloaded 11/28/21 12:39 AM UTC

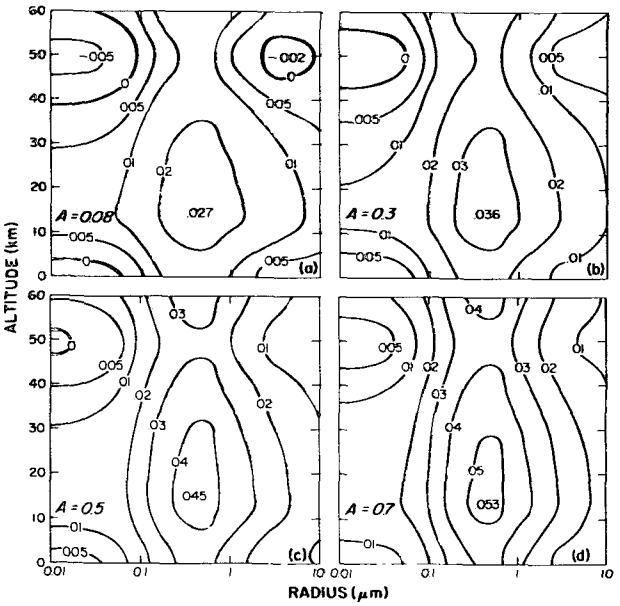

FIG. 3. Summertime heating rates (K day^{-1}) for aerosols with a constant mass mixing ratio of 1 ppb for 45°N at midday for (a) $A=0.08$, (b) $A=0.3$, (c) $A=0.5$ and (d) $A=0.7$.

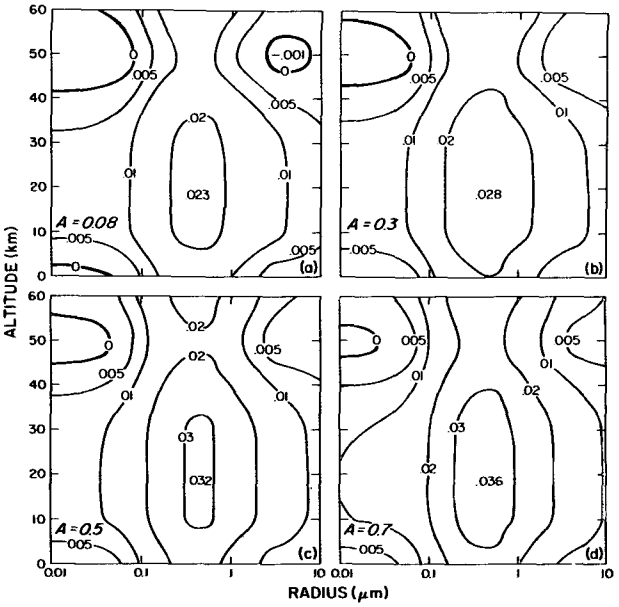

FIG. 4. As in Fig. 3 except for wintertime heating rates.

value in summer. Moreover, at low values of the albedo, negative heating rates are also obtained around 50 km for particles with radii larger than about 2 μm, and in the lower troposphere for particles with radii smaller than about 0.05 μm. Fig. 5 shows nighttime heating rates for (a) summer and (b) winter—indicating heat removal at any altitude and for each value of the particle radius, with the exception of a limited region just above the tropopause in summer for particles with radii larger than about 3 μm.

Using the procedures described in FGV, we computed daily averaged heating rates for summer and winter and for different albedo values. These are shown in Figs. 6 and 7. On the basis of these figures we can draw some conclusions about the role of aerosols at temperate latitudes. There is a large variation of the heating rate as a function of height and particle radius; it is apparent that particles of about 0.5 μm radius would be the most active in heating the ambient gas. In the region of the atmosphere around the stratopause, the aerosols would almost always remove heat, although their concentrations at those heights are normally so small that the process may not be important. In the lower stratosphere where the photochemical heating terms are minimal, and where the aerosols are abundant, they always add heat. The heat exchange varies with the albedo; thus, a coupling mechanism exists between the earth's surface and the stratosphere which may have effects on the stratospheric climate. In the low troposphere, the aerosols would almost always remove heat during the wintertime, and may also remove heat during the summertime in regions which have low albedo values.

In the above computations, the accommodation coefficient was assumed to have the value $a=1$. The

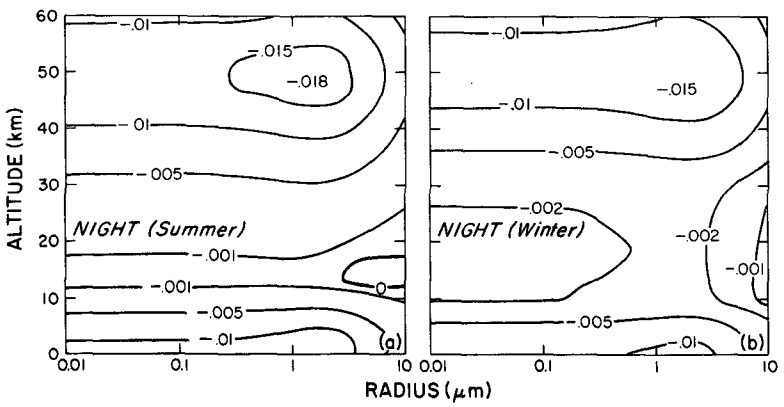

FIG. 5. Nighttime heating rates (K day^{-1}) for aerosols with a constant mass mixing ratio of 1 ppb for 45°N for (a) summer and (b) winter.

Unauthenticated | Downloaded 11/28/21 12:39 AM UTC

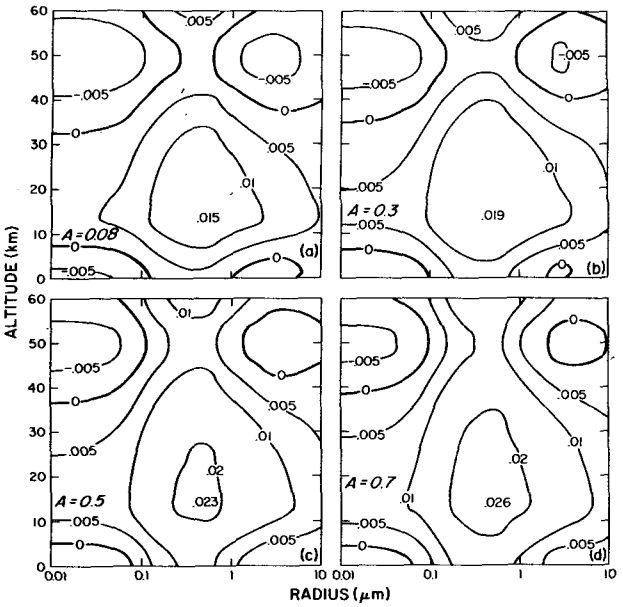

FIG. 6. Daily average heating rates (K day^{-1}) for aerosols with a constant mass mixing ratio of 1 ppb at 45°N for summer conditions with (a) $A=0.08$, (b) $A=0.3$, (c) $A=0.5$ and (d) $A=0.7$. The $A=0.3$ values are thought to best represent summertime conditions.

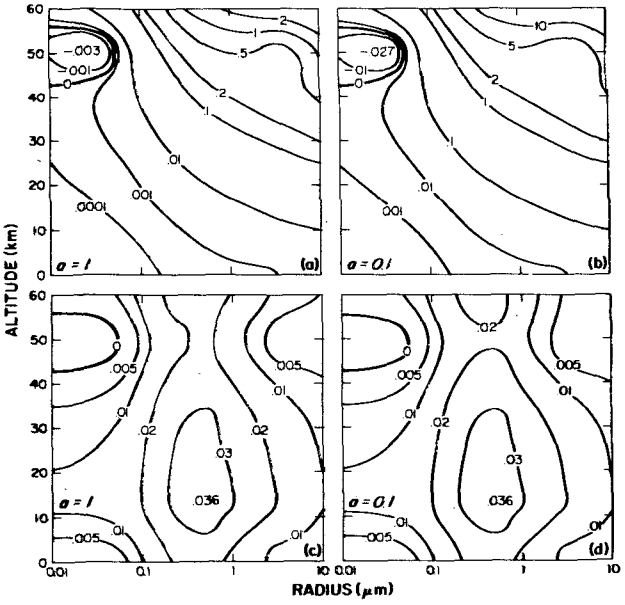

FIG. 8. Effect of accommodation coefficient on temperature differences and heating rates calculated for summertime midday conditions at 45°N with $A=0.3$ for aerosols with a constant mass mixing ratio of 1 ppb. Temperature differences T_p-T_g are shown for (a) $a=1$ and (b) $a=0.1$. Heating rates dT_g/dt are shown for (c) $a=1$ and (d) $a=0.1$.

effect of using smaller values of a can be deduced by considering the terms in the equilibrium condition (1). With the use of Eqs. (2) through (5), incremental analysis shows that decreasing the value of a will increase the particle temperature T_p. However, the first two terms in (1), $P_{A,\odot}$ and $P_{A,\mathrm{pla}}$, will not change as a is varied. Furthermore, when temperature differences T_p-T_g are very small (e.g., 1 K or less), P_E will be almost equal to the power radiated by the particle at the temperature of the gas T_g. Thus, the value of P_C does not vary appreciably as a is varied. It thereby follows from (5) that the temperature difference T_p-T_g will be inversely proportional to a; thus, for example, decreasing the accommodation coefficient by a factor of 2 would double the value of T_p-T_g as long as $T_p\approx T_g$. On the other hand, since P_C remains almost constant, (10) shows that the heating rate will be nearly independent of a under the same condition.

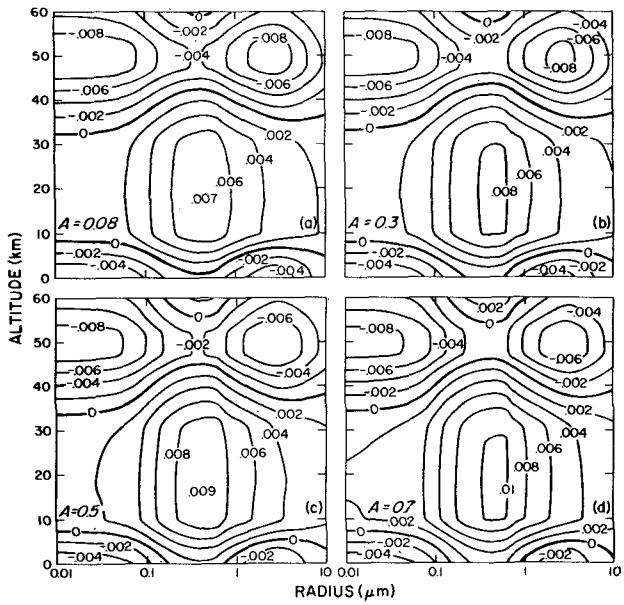

FIG. 7. As in Fig. 6 except for winter. The $A=0.5$ values are thought to best represent wintertime conditions.

These conclusions are demonstrated in Fig. 8, which compares temperature differences and heating rates obtained using $a=0.1$ with those obtained for $a=1$. Part (a) shows temperature differences calculated for summertime conditions at 45°N at midday with $A=0.3$ using $a=1$ for the accommodation coefficient; part (b) shows the results of changing the accommodation coefficient to $a=0.1$ for the same calculations. The values of the temperature difference contours in part (b) are almost 10 times those shown in part (a)—as was predicted in the above discussion for the situation in which $T_p\approx T_g$. Parts (c) and (d) show the heating rates associated with the above T_p-T_g calculations using $a=1$ and $a=0.1$, respectively. With the exception of the heating rates for the largest particle radii at the highest altitudes (50 km and above), the results appear to be identical. We conclude that, although the temperature difference values would be sensitive to our choice of accommodation coefficient, the heating rates calculated in the present study will not be significantly altered whatever value of a is chosen.

Unauthenticated | Downloaded 11/28/21 12:39 AM UTC

For the heating rate computations, a constant aerosol mass mixing ratio, $\nu=1$ ppb, has been assumed. In the lower troposphere, concentrations often exceed that value; in most other regions, however, they are normally lower. Regarding stratospheric aerosols, it is known that the aerosol mass concentration is variable, and that it often exceeds the above value—especially after major volcanic eruptions. In order to relate our results to observational data, we should like to make reference to the stratospheric aerosol measurements obtained with optical radars, and to relate the backscattering cross sections thus obtained to the aerosol mass mixing ratio.

The optical radar (also called laser radar or *lidar*, an acronym for *li*ght *d*etection *a*nd *r*anging) is by now a standard technique for studying the aerosol content of the atmosphere—particularly at stratospheric heights. The lidar technique provides data on the ratio δ between the volume backscattering coefficient of the aerosols and that of the molecular constituents.

At times subsequent to volcanic eruptions, δ may attain values exceeding unity at stratospheric altitudes. Such high ratios were observed in the 10–25 km altitude region after the eruption of Mt. Agung on Bali on 17 March 1963 (Fiocco and Grams, 1964; Grams and Fiocco, 1967) and after the eruption of Volcán de Fuego in Guatemala on 14 October 1974 (Fegley and Ellis, 1975; F. G. Fernald, personal communication, 1975; McCormick and Fuller, 1975). In order to relate the present results to laser radar observations, we have computed the daily average heating rates that would ensue if δ were exactly equal to unity at all altitudes.

Fig. 14 of FGV shows the mass mixing ratio ν of aerosols required to produce equal aerosol and molecular backscattering ($\delta=1$) for the wavelength 0.694 μm (as with a ruby-laser radar) for the synthetic aerosol model—assuming an aerosol mass density $\rho_p=1$ g cm^{-3}. This result showed that for $\delta=1$, ν generally exceeds 1 ppb by factors varying from about 1 to more than 1000 over the size range 0.01 to 10 μm radius. For the present study we have used smoothed values of ν, as shown in Fig. 9. For consistency with the spectral variation of the complex refractive index specified by Ivlev and Popova, we have used their value, $n=1.65-0.005i$, for the aerosol refractive index at the laser wavelength, $\lambda=0.694$ μm; these results are shown as curve (a). For reference, curve (b) shows the same computation for a value $n=1.525-0.005i$. This second value of n is regarded as more representative of the atmospheric aerosol—based on refractive index studies of soil-particle aerosols near the earth's surface (Grams *et al.*, 1974) and on some of our unpublished data for aerosols located in the troposphere and lower stratosphere, obtained with an aerosol-optics measurement system

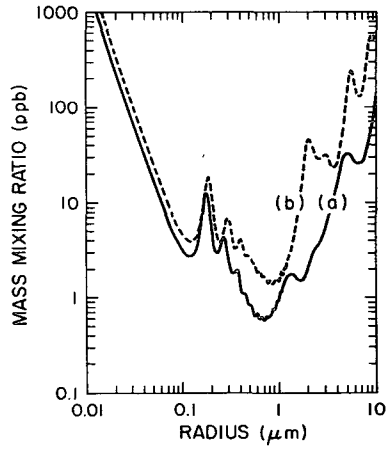

FIG. 9. Smoothed values of the mass mixing ratio of aerosols required to produce equal molecular and aerosol backscattering ($\delta=1$) at 0.694 μm wavelength for (a) $n=1.65-0.005i$, the synthetic aerosol model of Ivlev and Popova used for the present calculations, and (b) $n=1.525-0.005i$.

flown aboard the NASA Convair 990 Airborne Laboratory (Grams *et al.*, 1975).

It is seen by inspection of Fig. 9(b) that a smaller value of the real refractive index leads to somewhat larger mass mixing ratios. As indicated above, however, we have used the values in Fig. 9(a) to maintain consistency with the complex refractive index used for the energetic equilibrium calculations.

The daily averaged heating rates for a constant ruby-laser lidar backscattering ratio $\delta=1$ are shown in Figs. 10 and 11 for summer and winter, respectively, and for different values of the albedo A. With reference to the 10 to 25 km altitude region, in which the stratospheric aerosol layer is located at temperature latitudes, a wide range of heating rates is observed. These values vary from as little as 0.004 K day^{-1}, for particles of about 0.7 μm radius during the wintertime, to more than 10 K day^{-1} for particles of 0.01 μm radius during the summertime. Representative particle sizes for stratospheric aerosols are, however, generally considered to be in the 0.1 to 0.3 μm radius interval for which daily average heating rates of order 0.05–0.1 K day^{-1} have been calculated. In the radius interval specified above, the summertime results (Fig. 10) show maximum values of about 0.15–0.25 K day^{-1} at about 0.2 μm radius, whereas the wintertime results (Fig. 11) show maximum values of about 0.07–0.1 K day^{-1} at the same particle size.

5. Conclusions

In assessing the heating effect of aerosols on the atmosphere, we have not taken into account that fraction of the emitted power P_E which is later absorbed by the atmosphere or by the surface. We have not considered the effects of clouds or other surface features on the planetary flux, nor variations in atmo-

Unauthenticated | Downloaded 11/28/21 12:39 AM UTC

spheric composition (which would have the most significant effect at night since the $P_{A,\odot}$ term always exceeds the $P_{A,\text{pla}}$ term in daytime). We have furthermore limited the present study to aerosols characterized by the complex refractive index model of Ivlev and Popova. Other approximations are involved in the assumption that the atmosphere is perfectly transparent for solar radiation; furthermore, no multiple scattering for such radiation has been considered. Also, the accommodation coefficient for the collisional exchange process has been taken equal to unity. These various points will be subjected to future analysis.

While the present model has adopted a more realistic representation of the spectral variability of the complex refractive index than has been used by other investigators to date, we plan additional future calculations for a number of different substances that have special significance for the stratospheric aerosol layer—such as sulphuric acid droplets and particles of volcanic ash. In particular the calculations have indicated that daily averaged atmospheric heating rates associated with the stratospheric aerosol layer in the 15 to 25 km altitude interval were likely to have been somewhere near 0.1 K day^{-1} after the eruption of Mt. Agung in 1963 and after the eruption of the Fuego volcano in 1974. These calculations apply to the atmosphere at 45°N. The results of Cadle *et al.* (1976) indicate that aerosol concentrations at the latitudes of the Agung and Fuego volcanos could have been an order of magnitude higher than those observed at 45°N during the first year or so after each eruption (i.e., $\delta \gtrsim 10$). Thus, heating rates of order 1 K day^{-1} would be expected in the equatorial regions following the above-mentioned volcanic eruptions. The distribution with longitude and latitude of stratospheric temperature increases observed after the eruption of Mt. Agung (Newell, 1971) is highly correlated with the geographical distribution of albedo measured by Raschke *et al.* (1973). Thus, we also plan to relate the heating rates calculated for stratospheric particulates to temperature changes observed after known incursions of volcanic material into the stratosphere.

The present analyses have provided us with new insights into the effect of aerosols on the climate or, more specifically, on the radiation balance of the Earth-atmosphere system. In existing models their effect has customarily been divided into a reduction

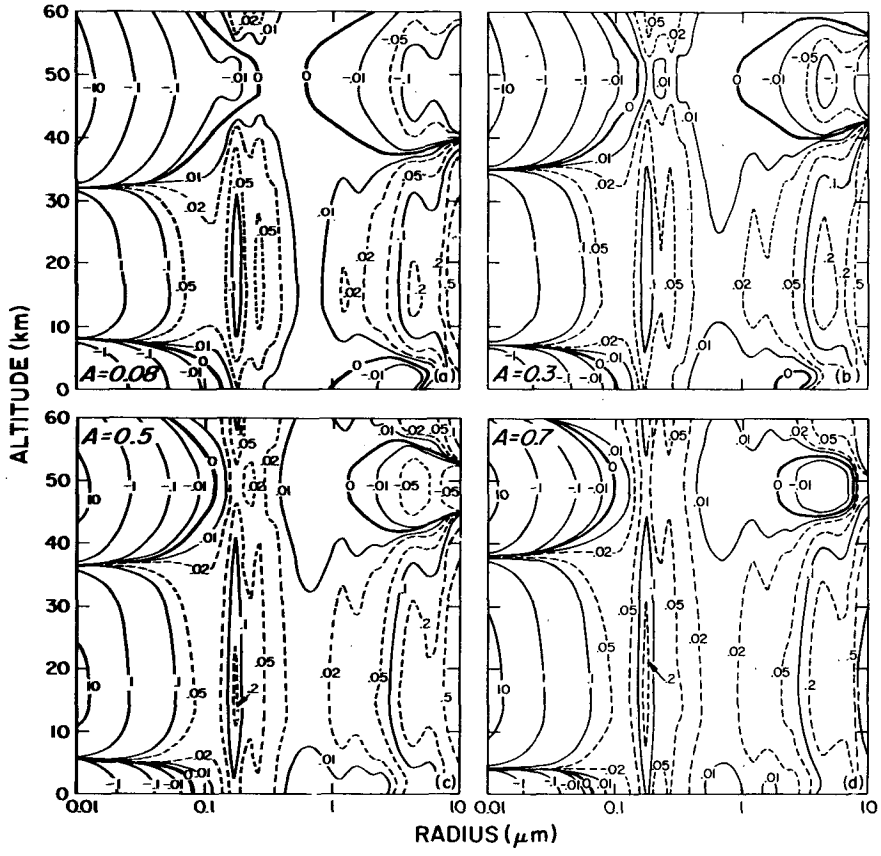

FIG. 10. Daily average heating rates (K day^{-1}) for aerosols having laser backscattering ratios $\delta=1$ at 45°N for summer with (a) $A=0.08$, (b) $A=0.3$, (c) $A=0.5$ and (d) $A=0.7$. These results are obtained by multiplying the heating rates presented in Fig. 6 by the mixing ratios shown in curve (a) of Fig. 9.

Unauthenticated | Downloaded 11/28/21 12:39 AM UTC

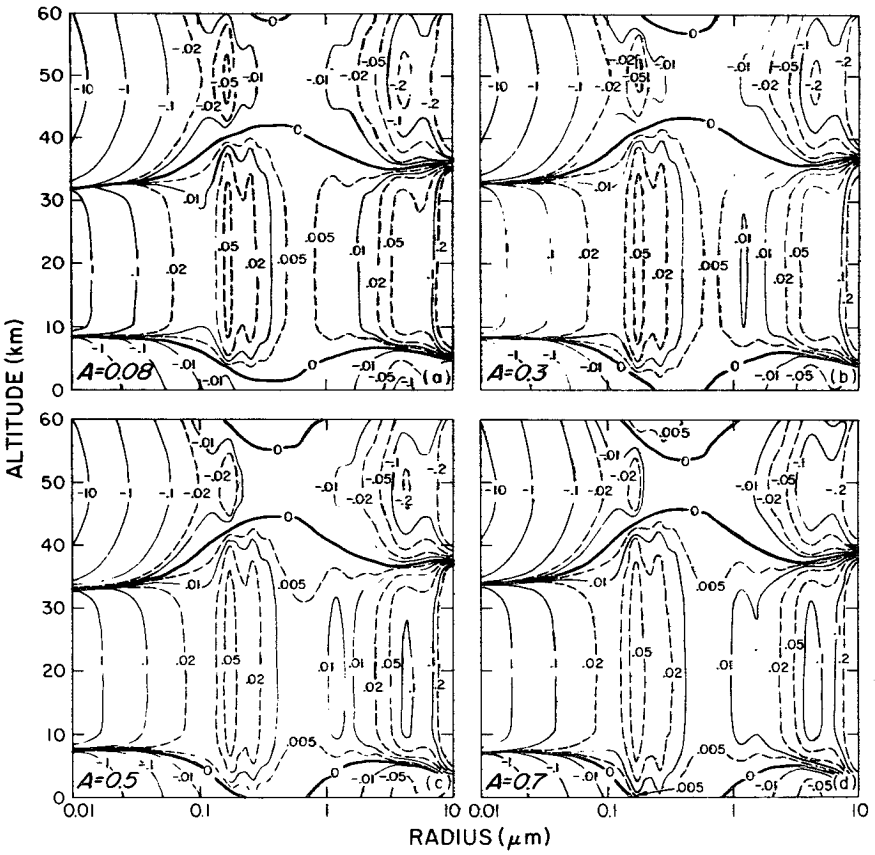

FIG. 11. As in Fig. 10 except for winter. These results are obtained by multiplying the heating rates presented in Fig. 7 by the mixing ratios shown in curve (a) of Fig. 9.

of the solar flux incident at the planetary surface and the *in situ* heating associated with the absorption of solar radiation by the aerosols; long-wave radiation has generally been neglected. In spite of the limitations placed on the analysis by our assumptions, the present account of the absorption aspect of this problem may provide additional information for use in modelling the climatic impact of atmospheric aerosols.

Acknowledgment. The authors wish to thank Diran Deirmendjian and James A. Coakley, Jr., for their helpful comments and suggestions.

REFERENCES

Bignell, K. J., 1970: The water-vapor infrared continuum. *Quart. J. Roy. Meteor. Soc.*, **96**, 390–403.

Cadle, R. D., C. S. Kiang and J.-F. Louis, 1976: The global-scale dispersion of the eruption clouds from major volcanic eruptions. *J. Geophys. Res.*, **81**, 3125–3132.

Cox, S. K., 1973: Infra-red calculations with a water vapor pressure broadened continuum. *Quart. J. Roy. Meteor. Soc.*, **99**, 669–679.

Fiocco, G., G. Grams and G. Visconti, 1975: Equilibrium temperature of small particles in the upper atmosphere (50–110 km). *J. Atmos. Terr. Phys.*, **37**, 1327–1337.

——, and G. Visconti, 1973: On the seasonal variation of upper atmospheric sodium. *J. Atmos. Terr. Phys.*, **35**, 165–171.

——, and G. Grams, 1964: Observations of the aerosol layer at 20 km by optical radar. *J. Atmos. Sci.*, **21**, 323–324.

Fegley, R. W., and H. T. Ellis, 1975: Lidar observations of a stratospheric dust layer in the tropics, *Geophys. Res. Lett.*, **2**, 139–142.

Grams, G., and G. Fiocco, 1967: Stratospheric aerosol layer during 1964 and 1965. *J. Geophys. Res.*, **72**, 3523–3541.

——, and ——, 1976: Equilibrium temperatures of spherical ice particles in the upper atmosphere and implications for noctilucent cloud formation. *J. Geophys. Res.* (in press).

——, I. H. Blifford, Jr., D. A. Gillette and P. B. Russell, 1974: Complex refractive index of airborne soil particles. *J. Appl. Meteor.*, **13**, 459–471.

——, A. J. Dascher and C. M. Wyman, 1975: Airborne laser polar nephelometer for airborne measurements of aerosol optical properties. *Opt. Eng.*, **14**, 85–90.

Higuchi, K., 1969: Growth of ice crystals under radiative cooling. *J. Meteor. Soc. Japan*, **47**, 446–449.

Ivlev, L. S., and S. I. Popova, 1973: The complex refractive indices of substances in the atmospheric-aerosol dispersed phase. *Izv. Atmos. Oceanic Phys.*, **9**, 1034–1043.

Kennard, E. H., 1938: *Kinetic Theory of Gases.* McGraw-Hill, Inc., 483 pp.

Kunde, V. G., B. J. Conrath, R. A. Hanel, W. C. Maguire, C. Prabhakara and V. V. Salomonson, 1974: The Nimbus 4 infrared spectroscopy experiment 2. Comparison of observed and theoretical radiances from 425–1450 cm^{-1}. *J. Geophys. Res.*, **79**, 777–789.

Unauthenticated | Downloaded 11/28/21 12:39 AM UTC

McCormick, M. P., and W. H. Fuller, Jr., 1975: Lidar measurements of two intense stratospheric dust layers. *Appl. Opt.*, **14**, 4–5.

Newell, R. E., 1971: The global circulation of atmospheric pollutants. *Sci. Amer.*, **224**, 32–42.

Raschke, E., T. H. Vonder Haar, W. R. Bandeen and M. Pasternak, 1973: The annual radiation balance of the earth-atmosphere system during 1969–70 from Nimbus 3 measurements. *J. Atmos. Sci.*, **30**, 341–364.

Rodgers, C. D., 1968: Some extensions and applications of the new random model for molecular band transmission. *Quart. J. Roy. Meteor. Soc.*, **94**, 99–102.

——, and C. D. Walshaw, 1966: The computation of infrared cooling rate in planetary atmospheres. *Quart. J. Roy. Meteor. Soc.*, **92**, 67–92.

Shifrin, K. S., and Zh. K. Zolotova, 1966: Kinetics of the evaporation of drops in a radiation field. *Izv. Atmos. Oceanic Phys.*, **2**, 1311–1315.

——, and ——, 1971: The growth kinetic of a drop in the radiation field of the earth and atmosphere. *Izv. Atmos. Oceanic Phys.*, **7**, 228–231.

Thekaekara, M. P., 1973: Solar energy outside the earth's atmosphere. *Solar Energy*, **14**, 109–127.

Unauthenticated | Downloaded 11/28/21 12:39 AM UTC